Nonlinear ultrafast optical absorption and pump-probe spectroscopy in biased semiconductor superlattices

Lijun Yang and Marc M. Dignam
Department of Physics, Queen's University, Kingston, Ontario, Canada K7L 3N6
(Received 12 October 2005; published 31 January 2006)

We present theoretical simulations of two important nonlinear optical phenomena in biased semiconductor superlattices: nonlinear ultrafast absorption and pump-probe spectroscopy. We find that for both these techniques, the excitonic Wannier-Stark ladder absorption peaks shift as the optical intensity is increased. We show that both of these measurements can be used to probe the ultrafast internal intraband electric field within the superlattice. We employ a nonperturbative formalism in an excitonic basis to model the dynamic response. This allows us to self-consistently include the self-generated internal intraband field that generates the spectral peak shifts.

DOI: 10.1103/PhysRevB.73.035334 PACS number(s): 78.67.Pt, 42.65.Re, 78.40.−q, 78.67.−n

I. INTRODUCTION

Linear and nonlinear absorption spectroscopy can provide invaluable information on both the electronic states and the ultrafast dynamics in bulk semiconductors and their heterostructures.[1] For simple atomic systems, the calculation of the *linear* optical response is relatively straightforward; however, for semiconductor nanostructures, it can be very complicated,[2–7] as the response often involves factors such as excitonic effects,[8,9] continuum states,[9–16] and multiband interactions.[9,15]

The calculation of the *nonlinear* optical response in semiconductors is much more difficult than the linear response; it is generally dominated by many-body Coulomb correlations[17–19] that result in a high sensitivity to excitation intensities (carrier densities). Various many-body effects such as dynamic screening, local-field effects, exchange-correlation-induced band-gap renormalization, and phase-space filling (PSF) effects often play important roles in the nonlinear optical response of semiconductors.[20–23] In many cases, one or two particular many-body correlations dominate the nonlinear optical response and lead to obvious density-dependent spectral peak shifts. In other cases, however, different many-body effects can compensate or cancel each other and lead to density-independent spectral peak positions.[24,25] Often, to accurately account for experimental results, the treatment of the nonlinear optical response of semiconductors has to be *nonperturbative* in the optical field,[26–30] as perturbative methods are only valid for low excitation levels.[31]

In this work, we model the ultrafast nonlinear optical response of an important semiconductor heterostructure: a biased semiconductor superlattice (BSSL). A BSSL is an excellent model system to investigate theoretical approaches to the ultrafast coherent dynamics and spectroscopy of semiconductor heterostructures such as asymmetric or biased coupled multiple-quantum-well structures, where both interband and intraband dynamics play important roles.

In a single-particle picture, the electronic eigenstates of a BSSL in the presence of an external dc field F_o are given by $E_n=E_0+neF_od$, where d is the lattice period, F_o is the applied dc field and n is an integer.[32–34] These eigenstates form the so-called Wannier-Stark Ladder (WSL); Bloch oscillations[35,36] (BO's) occur when wave packets formed from these WSL states are generated, for example, by an ultrashort optical pulse. The wave packets oscillate at the BO frequency, which is given by $\omega_B \equiv eF_od/\hbar$. Due to the strong interaction between the interband and intraband polarizations, the WSL is renormalized for moderate to high optical excitations; this considerably modifies the system dynamics. In previous work, it has been shown both experimentally and theoretically that the effect of the intraband field on the WSL can be seen from spectrally resolved four-wave mixing experiments[37–41] and from the density dependence of the THz emission frequency generated by BO's.[31] These four-wave mixing experiments are very difficult to perform, model, and interpret, and the THz experiments require complex THz collection and detection apparatus. It would therefore be advantageous to have other optical methods with which to probe the internal intraband field of the BSSL.

In this work, we investigate the ultrafast nonlinear absorption and pump-probe spectra of BSSL's and show that they can both be used to determine the internal intraband field of the BSSL. The calculation of the optical response of BSSL's is computationally very intensive; it is impossible to simulate either the linear or nonlinear optical response of BSSL's with the sort of few-level model that is often employed in modeling the nonlinear optical response of quantum wells. When moderate to high bias fields are applied to BSSL's (usually larger than 5 kV/cm), the number of basis states required to accurately account for experimental results is at least on the order of 10^3. To keep the calculation tractable while still capturing the main features of the system dynamics such as dynamic screening,[24,42–51] we employ our nonperturbative excitonic Bloch equations[31,40] to calculate the nonlinear optical response. Because the nonlinear response arising from Pauli blocking or phase-space filling effects is usually small in semiconductors[17,25] as compared to Coulomb correlations, PSF effects are neglected in our current formalism.

We find that the WSL optical absorption peaks show blueshifts or redshifts as the excitation density increases, depending on whether a specific peak is below or above the $n=0$ $1s$

excitonic WSL state. The pump-probe absorption spectra also show obvious density-dependent spectral peak shifts that can be used to accurately monitor the instantaneous internal field of the photoexcited BSSL.

The paper is organized as follows. In Sec. II, we present our nonperturbative formalism for calculating the interband and intraband dynamics and the nonlinear absorption spectra of BSSL's. In Secs. III and IV, simulations of nonlinear optical absorption and pump-probe spectroscopy in a BSSL are presented. Finally, in Sec. V, we summarize our findings.

II. THEORY

Treating the exciton-exciton interaction in the long-wavelength dipole approximation, the second-quantized Hamiltonian of a BSSL in an exciton basis takes the form[31,40,41]

$$H = \sum_{\mu} \sum_{\mathbf{K}=\{\mathbf{K}_1,\mathbf{K}_2\}} \hbar\omega_{\mu} B^{\dagger}_{\mu,\mathbf{K}} B_{\mu,\mathbf{K}} + V\left(-\mathbf{E}_{\mathrm{opt}}\cdot\mathbf{P}_{\mathrm{inter}} + \frac{1}{2\epsilon_0\epsilon_b}\mathbf{P}_{\mathrm{intra}}\cdot\mathbf{P}_{\mathrm{intra}}\right), \tag{1}$$

where ϵ_0 is the vacuum permittivity, V is the volume of the system, and $B^{\dagger}_{\mu,\mathbf{K}}(B_{\mu,\mathbf{K}})$ is the creation (annihilation) operator for a WSL exciton in the dc field, with internal quantum number μ, center-of-mass wave vector $\mathbf{K}$, and energy $\hbar\omega_{\mu}$. We have neglected the dependence of $\omega_{\mu,\mathbf{K}}$ on $\mathbf{K}$, as this is negligible, given that the $\mathbf{K}$ are given by the optical photon momenta. The quantity ϵ_b is the dielectric constant, which accounts for the background screening of the Coulomb interaction due to all off-resonant contributions that are not explicitly taken into account.[52] The optical field consists of a strong pump pulse propagating in the $\mathbf{K}_1$ direction, followed by a very weak probe pulse propagating in the $\mathbf{K}_2$ direction; it takes the form

$$\mathbf{E}_{\mathrm{opt}}(t) = \mathbf{E}^{(1)}_{\mathrm{opt}}(t) + \mathbf{E}^{(2)}_{\mathrm{opt}}(t-\tau), \tag{2}$$

where ω_c is the central laser frequency, τ is the delay time of the probe pulse relative to the pump pulse, and

$$\mathbf{E}^{(j)}_{\mathrm{opt}}(t) = \boldsymbol{\mathcal{E}}^{(j)}(t)e^{-i\omega_c t} + \mathrm{c.c.}.$$

is the optical field of the pump [probe] pulse for $j=1$ [$j=2$]. The function $\boldsymbol{\mathcal{E}}^{(1)}(t)$ [$\boldsymbol{\mathcal{E}}^{(2)}(t)$] is optical pulse envelope for the pump [probe] field.

The polarization operator is defined as

$$\mathbf{P} \equiv \mathbf{P}_{\mathrm{inter}} + \mathbf{P}_{\mathrm{intra}}, \tag{3}$$

where $\mathbf{P}_{\mathrm{inter}}$ and $\mathbf{P}_{\mathrm{intra}}$ denote, respectively, the interband and intraband polarizations. The interband polarization is defined as

$$\mathbf{P}_{\mathrm{inter}} \equiv \frac{1}{V}\sum_{\mu}\sum_{\mathbf{K}=\{\mathbf{K}_1,\mathbf{K}_2\}} [\mathbf{M}_{\mu} B^{\dagger}_{\mu,-\mathbf{K}} + \mathbf{M}^{*}_{\mu} B_{\mu,\mathbf{K}}], \tag{4}$$

where $\mathbf{M}_{\mu}$ is the interband dipole matrix element of the μth excitonic state $|\psi^{\mu}\rangle$. The intraband polarization is given by

$$\mathbf{P}_{\mathrm{intra}} \simeq \mathbf{P}^{(1)}_{\mathrm{intra}} \equiv \frac{1}{V}\sum_{\mu,\mu'} \mathbf{G}_{\mu,\mu'} B^{\dagger}_{\mu,\mathbf{K}_1} B_{\mu',\mathbf{K}_1}, \tag{5}$$

where $\mathbf{G}_{\mu\mu'}$ is the intraband dipole matrix element between two excitonic states $|\psi^{\mu}\rangle$ and $|\psi^{\mu'}\rangle$. In calculating the intraband polarization, we have included only the portion arising from the pump pulse, because the probe pulse is very weak. Detailed derivations of these expressions are given in our earlier work.[40,41]

We first present the dynamic equations for the excitons that are generated by the pump pulse—i.e., those with center-of-mass wave vector $\mathbf{K}_1$. These dynamic equations are treated nonperturbatively in the optical field and take the form

$$i\hbar\frac{d\langle B^{\dagger}_{\mu,\mathbf{K}_1}\rangle}{dt} + \hbar\left(\omega_{\mu} + \frac{i}{T_{\mu}}\right)\langle B^{\dagger}_{\mu,\mathbf{K}_1}\rangle = \mathbf{E}^{(1)}_{\mathrm{opt}}(t)\cdot\mathbf{M}^{*}_{\mu} + \mathbf{E}^{(1)}_{\mathrm{intra}}\cdot\sum_{\mu'}\mathbf{G}_{\mu',\mu}\langle B^{\dagger}_{\mu',\mathbf{K}_1}\rangle \tag{6}$$

and

$$\begin{aligned} i\hbar\frac{d\langle B^{\dagger}_{\mu,\mathbf{K}_1}B_{\nu,\mathbf{K}_1}\rangle}{dt} = &-\hbar\left(\omega_{\mu}-\omega_{\nu}+\frac{i}{T_{\mu\nu}}\right)\langle B^{\dagger}_{\mu,\mathbf{K}_1}B_{\nu,\mathbf{K}_1}\rangle \\ &+ \mathbf{E}^{(1)}_{\mathrm{opt}}(t)\cdot[\mathbf{M}^{*}_{\mu}\langle B_{\nu,\mathbf{K}_1}\rangle - \mathbf{M}_{\nu}\langle B^{\dagger}_{\mu,\mathbf{K}_1}\rangle] \\ &+ \mathbf{E}^{(1)}_{\mathrm{intra}}\cdot\sum_{\mu'}(\mathbf{G}_{\mu',\mu}\langle B^{\dagger}_{\mu',\mathbf{K}_1}B_{\nu,\mathbf{K}_1}\rangle \\ &- \mathbf{G}^{*}_{\mu',\nu}\langle B^{\dagger}_{\mu,\mathbf{K}_1}B_{\mu',\mathbf{K}_1}\rangle). \end{aligned} \tag{7}$$

A phenomenological interband dephasing time constant $T_{\mu} = T_{2inter}$ is added to Eq. (6). The time constant $T_{\mu\nu}$ in Eq. (7) is the intraband dephasing constant T_{2intra} when $\mu \neq \nu$ and is the exciton population lifetime T_{1ex} when $\mu=\nu$. The self-induced intraband electric field $\mathbf{E}^{(1)}_{\mathrm{intra}}$ in Eq. (7) arises from the excitons excited by the pump pulse and is defined as

$$\mathbf{E}^{(1)}_{\mathrm{intra}}(t) \equiv -\frac{1}{\epsilon_0\epsilon_b}\langle\mathbf{P}^{(1)}_{\mathrm{intra}}\rangle. \tag{8}$$

To close the infinite hierarchy of dynamic equations encountered in the derivation of Eqs. (6) and (7), we have employed the following factorizations:

$$\langle B^{\dagger}_{\mu'',\mathbf{K}_1}B_{\mu''',\mathbf{K}_1}B^{\dagger}_{\mu',\mathbf{K}_1}\rangle = \langle B^{\dagger}_{\mu'',\mathbf{K}_1}B_{\mu''',\mathbf{K}_1}\rangle\langle B^{\dagger}_{\mu',\mathbf{K}_1}\rangle, \tag{9}$$

$$\langle B^{\dagger}_{\mu'',\mathbf{K}_1}B_{\mu''',\mathbf{K}_1}B^{\dagger}_{\mu',\mathbf{K}_1}B_{\nu,\mathbf{K}_1}\rangle = \langle B^{\dagger}_{\mu'',\mathbf{K}_1}B_{\mu''',\mathbf{K}_1}\rangle\langle B^{\dagger}_{\mu',\mathbf{K}_1}B_{\nu,\mathbf{K}_1}\rangle. \tag{10}$$

Note that these factorizations are crucial in enabling us to include Coulomb correlations between electrons and holes beyond a first-order cluster expansion.[42] For example, the factorization in Eq. (9) roughly corresponds to the factorization of a six-point electron-hole correlation function into the product of four-point and two-point electron-hole correlation functions. This obviously goes beyond the factorization of a four-point electron-hole correlation function into the product of two two-point electron-hole correlation functions in the

first-order semiconductor Bloch equations.[26] The crucial feature of our approach is that the use of the exciton basis reduces enormously the computational effort needed, while still capturing the key features of the system dynamics that would be lost in a perturbative expansion in the optical field.[31]

To calculate the pump-probe spectra, we need another dynamic equation describing the interband dynamics of the excitons generated by the probe pulse; this takes the form

$$i\hbar\frac{d\langle B^{\dagger}_{\mu,\mathbf{K}_2}\rangle}{dt} = -\hbar\left(\omega_\mu + \frac{i}{T_\mu}\right)\langle B^{\dagger}_{\mu,\mathbf{K}_2}\rangle + \mathbf{E}^{(2)}_{\mathrm{opt}}(t-\tau)\cdot\mathbf{M}^{*}_{\mu} + \mathbf{E}^{(1)}_{\mathrm{intra}}\cdot\sum_{\mu'}\mathbf{G}_{\mu',\mu}\langle B^{\dagger}_{\mu',\mathbf{K}_2}\rangle. \quad (11)$$

Note that the response to the probe pulse is treated only to first order in the probe optical field in Eq. (11) due to its much weaker intensity as compared to the pump pulse. It is possible to go beyond this approximation, as we have done in calculating the degenerate four-wave mixing (DFWM) signal in a previous publication.[40] However, this complicates the calculations enormously, as one has to sum over many different diffraction orders in order to achieve convergence. As a result, such nonperturbative DFWM calculations have only been performed with a basis consisting of only $1s$ excitons. The current work is the first nonperturbative calculation of the pump-probe signal from a BSSL in an excitonic basis. Using a weak pump pulse not only simplifies the calculation, but also simplifies the interpretation of the results, as there are no multi-diffracted excitons to complicate the spectra.[40]

To calculate either the nonlinear absorption or pump-probe spectra, we need to calculate the nonlinear interband polarization. In the nonlinear absorption experiments, there is only one pulse, the pump pulse. Thus we need first to solve Eqs. (6) and (7) for the pump pulse. Then we substitute the time-dependent solution of $\langle B^{\dagger}_{\mu,\mathbf{K}_1}\rangle$ into Eq. (4) to obtain the nonlinear interband polarization with wave vector $\mathbf{K}_1$. To calculate the pump-probe spectra, we need first solve the coupled nonlinear Eqs. (6), (7), and (11) for different time delays between pump and probe pulses, and then substitute the time-dependent solution of $\langle B^{\dagger}_{\mu,\mathbf{K}_2}\rangle$ into Eq. (4) to obtain the nonlinear interband polarization propagating with wave vector $\mathbf{K}_2$.

Now we present the formalism for calculating both the nonlinear absorption and pump-probe spectra of a BSSL using the calculated interband polarization. To do this, we first write the interband polarization propagating in the $\mathbf{K}_j$ direction ($j=\{1,2\}$) in the form

$$\mathbf{P}^{(j)}_{\mathrm{inter}}(t) = \mathbf{p}^{(j)}_{\mathrm{inter}}(t)e^{-i\omega_c t} + \mathrm{c.c.}, \quad (12)$$

where $\mathbf{p}^{(j)}_{\mathrm{inter}}(t)$ is the slowly varying envelope function of the interband polarization, which is given by

$$\mathbf{p}^{(j)}_{\mathrm{inter}}(t) = \frac{1}{V}\sum_{\mu}\mathbf{M}^{*}_{\mu}\langle B_{\mu,\mathbf{K}_j}\rangle(t)e^{i\omega_c t}.$$

The Fourier transform of the interband polarization is given by

$$\mathbf{P}^{(j)}_{\mathrm{inter}}(\omega-\omega_c) \equiv \int_{-\infty}^{\infty}[\mathbf{p}^{(j)}_{\mathrm{inter}}(t)e^{-i\omega_c t} + \mathrm{c.c.}]e^{-i(\omega-\omega_c)t}dt \cong \mathbf{p}^{(j)}_{\mathrm{inter}}(\omega), \quad (13)$$

where $\mathbf{p}^{(j)}_{\mathrm{inter}}(\omega)\equiv\int_{-\infty}^{\infty}\mathbf{p}^{(j)}_{\mathrm{inter}}(t)e^{-i\omega t}dt$. Therefore, the Fourier transform of the total interband polarization at $\omega-\omega_c$ is approximately equal to the Fourier transform of the envelope function of the interband polarization at ω. With exactly the same procedure, the Fourier transform of the laser pulse [Eq. (2)] can be written in the form

$$\mathbf{E}^{(j)}_{\mathrm{opt}}(\omega-\omega_c) \cong \int_{-\infty}^{\infty}\boldsymbol{\mathcal{E}}^{(j)}(t)e^{-i\omega t}dt \equiv \boldsymbol{\mathcal{E}}^{(j)}(\omega), \quad (14)$$

where $\boldsymbol{\mathcal{E}}^{(j)}(\omega)$ is the Fourier transform of the optical envelope function $\boldsymbol{\mathcal{E}}^{(j)}(t)$.

With the above definitions, the optical absorption $\alpha^{(j)}(\omega)$ is given by[53]

$$\alpha^{(j)}(\omega-\omega_c) = \frac{\omega_c}{n' c\epsilon_0}\,\mathrm{Im}\left[\frac{\mathbf{P}^{(j)}_{\mathrm{inter}}(\omega-\omega_c)\cdot\mathbf{E}^{(j)*}_{\mathrm{opt}}(\omega-\omega_c)}{|\mathbf{E}^{(j)}_{\mathrm{opt}}(\omega-\omega_c)|^2}\right] = \frac{\omega_c}{n' c\epsilon_0}\,\mathrm{Im}\left[\frac{\mathbf{p}^{(j)}_{\mathrm{inter}}(\omega)\cdot\boldsymbol{\mathcal{E}}^{(j)*}(\omega)}{|\boldsymbol{\mathcal{E}}^{(j)}(\omega)|^2}\right], \quad (15)$$

where n' is the average, frequency-independent refractive index of the BSSL and c is the speed of light.

In the dynamics calculations, $1s$ and higher in-plane excitonic states (HIES's) in the BSSL are all included in the basis. These states are calculated using the two-well excitonic states described in Ref. 10. The inclusion of HIES's is particularly important in modeling the dynamics in BSSL's; even in the low-exciton-density limit, the HIES's can qualitatively modify the intraband dynamics,[10] which in turn affects the absorption spectra.

Although the excitonic states are very complicated, for the convenience of discussion they can be approximately labeled by the index pair $\mu=(n,m)$, where n indicates the approximate WSL index of the exciton and m gives the dominant quantum number for in-plane motion. In this scheme, the intraband dipole of the (n,m) state in the z direction is approximately $-ned$, where $n=\ldots,-2,-1,0,1,2,\ldots$, as is the case for single-particle WSL states. The states with $m=1$ are $1s$-like excitonic states, while the states with $m>1$ correspond to HIES's, up to continuum states.

III. NONLINEAR OPTICAL ABSORPTION

We now calculate the nonlinear optical absorption of a BSSL. In this and all following sections, we model a $GaAs/Ga_{0.7}Al_{0.3}As$ superlattice with well width of 6.7 nm, barrier width of 1.7 nm, and bias field of 11.5 kV/cm. All other parameters used in the calculations are given in Ref. 8. The superlattice is excited with a transform-limited 86-fs Gaussian pulse with a spectral full width at half maximum (FWHM) of 21 meV and a central frequency $\omega_c=\omega_{(-1,1)}$, which corresponds to the $n=-1$ $1s$ excitonic WSL state (see

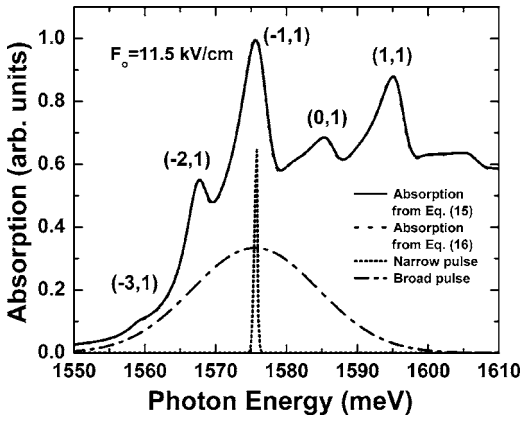

FIG. 1. Optical absorption spectra calculated using two different approaches in the low-excitation limit. Also shown are the two Gaussian pulses used in the nonlinear and pump-probe simulations. The spectrally broad pulse is the 86-fs probe pulse, and the spectrally narrow pulse is the pump pulse.

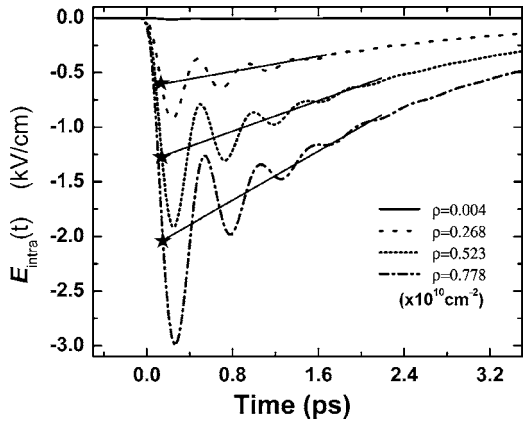

FIG. 2. The calculated intraband electric field as a function of time for different pump-induced exciton densities. The solid line in each curve shows schematically the decay of the average intraband field. The peak intraband field strengths used to calculate the F' used in the calculations presented in Fig. 3(b) are marked with stars.

the spectrally broad pulse in Fig. 1). The interband and intraband dephasing times are taken to be $T_{2inter}=0.34$ ps and $T_{2intra}=0.52$ ps, respectively, which are in agreement with those obtained in recent experiments on such a BSSL.[31] The exciton population lifetime is taken to be $T_{1ex}=2$ ps. The exciton lifetime here refers to the time that an exciton remains in a particular excitonic eigenstate; it is not the recombination time for an exciton, which is much longer. For the interband and intraband dephasing time constants chosen, we find that the precise value of T_{1ex} makes very little difference, as long it is longer than 1 ps.

Before calculating the nonlinear optical absorption spectra of the BSSL, we first consider the limiting case of very-low-intensity excitation, where the calculated nonlinear absorption spectra should be essentially identical to the linear optical spectra as calculated using the standard expression[8,10]

$$\alpha'(\omega)=\sum_{\mu}\frac{4\pi e^2|\boldsymbol{\xi}\cdot\mathbf{p}_{cv}|^2}{\omega m_0^2 n' c}\alpha_{\mu}\frac{\left(\frac{\Delta E}{2\pi}\right)}{(E-\hbar\omega)^2+\left(\frac{\Delta E}{2}\right)^2}. \quad (16)$$

In this equation, $\boldsymbol{\xi}$ is the electric field polarization vector, $\mathbf{p}_{cv}$ is the momentum matrix element between the bulk conduction-band and valence-band Bloch states at the band edges, m_0 is the free-electron mass, and α_{μ} is the absorption strength (which is proportional to $|\mathbf{M}_{\mu}|^2$).[8,10] In this expression, we have assumed Lorentzian line shapes with the same FWHM of ΔE for all excitonic states. This linewidth is directly related to the intraband dephasing used in the dynamics equations through the equation $\Delta E=1/(\pi T_{2inter})$. For the interband dephasing time chosen in this work, $T_{2inter}=0.34$ ps, and so we use $\Delta E=3.87$ meV.

As shown in Fig. 1, the absorption spectrum obtained by calculating the excitonic eigenstates and using Eq. (16) overlaps almost exactly with the one calculated by solving the dynamic equations and employing Eq. (15). The peak exciton areal density (peak density per superlattice period per unit area) is taken to be $\rho=0.004\times10^{10}$ cm^{-2}, and thus the induced intraband field is negligible ($\ll0.1$ kV/cm). The comparison above indicates the equivalence of the two methods for calculating linear optical absorption spectra in the BSSL. However, with Eq. (15), we can calculate both linear and nonlinear optical responses, with the linear response being the low-excitation limit.

We now turn to the calculation of the *nonlinear* absorption spectra in the BSSL by increasing optical intensity and hence the exciton density. In Fig. 2, we plot the intraband field $E_{intra}(t)\approx E_{intra}^{(1)}(t)$ as a function of time for excitation via the 86-fs optical pulse for four different peak densities (arising from different pulse intensities). As can be seen, the magnitude of the intraband field increases rapidly over the duration of the optical pulse and then decays slowly while oscillating. The initial rise in the field is due to the sudden creation of excitons with permanent intraband dipole moments [recall the $(-1,1)$ state has a dipole moment of roughly ed]. In BSSL's, the self-induced quasi-dc field generated by the excitonic dipoles always opposes the original external dc field and so is negative.[31] The field oscillations arise from the BO's of the superposition wave packet formed by the optical pulse. Finally, the slow decay in the dc component of the field is due to the population decay, while the decay in the ac portion is due to the intraband dephasing.

In Fig. 3(a), we plot the nonlinear absorption spectra for the same conditions used in Fig. 2. As the exciton density increases, due to higher optical excitation, it is obvious that the absorption peaks undergo either a blueshift or a redshift, depending whether a specific absorption peak is, respectively, below or above the (0,1) WSL state. The (0,1) WSL peak also initially undergoes a small blueshift, and then its oscillator strength essentially disappears. The oscillator strength corresponding to $(-2,1)$ and $(-1,1)$ states considerably increases and decreases, respectively, as the exciton density increases, while the oscillator strength corresponding to the (1,1) state remains approximately constant. All of this behavior can be understood by examining the field dependence of the excitonic WSL absorption spectrum.

The absorption peak shifts arise from the self-induced intraband electric field that considerably renormalizes the

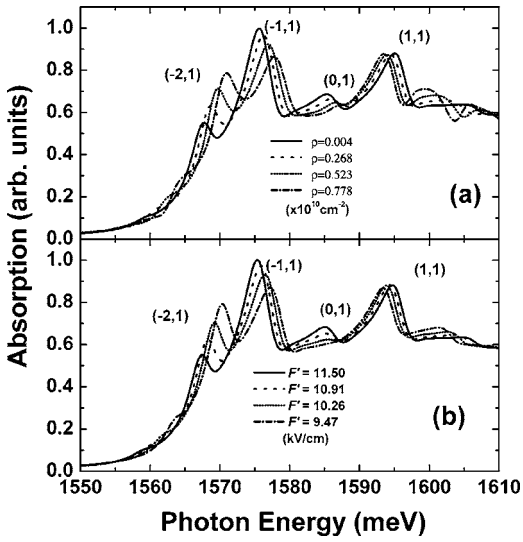

FIG. 3. (a) Nonlinear absorption spectra calculated for different densites, ρ, corresponding to different pulse intensities. (b). Linear absorption spectra calculated using different dc bias fields F' (in units of kV/cm) corresponding to the net bias field present just after the pulse arrives.

original WSL. Such an energy renormalization has been discussed previously in the context of four-wave mixing and THz radiation experiments.[31,37] Because the self-induced quasi-dc electric field always opposes the original external dc field, this leads to a reduction in the net bias field. Thus, as the density increases, the effective net bias field decreases and the spacing between the WSL levels decreases. We find that calculations taken only up to fourth order in the optical field drastically underestimate the spectral peak shifts (not shown). The calculations of the THz emission from a BSSL with perturbative methods up to fourth order in the optical field have been extensively investigated in Ref. 31, where we found that the fourth-order method was not accurate, leading to incorrect BO frequencies and overestimation of the THz radiation power.

Employing an exciton basis and treating the exciton dynamics nonperturbatively in the optical field amounts to treating the induced intraband electric field self-consistently in our formalism. This is essential in correctly interpreting experimental results because the induced intraband electric field renormalizes the system eigenstates instantly in the excitation process. Such an instant change in the self-induced intraband electric field must be fed back into dynamic equations simultaneously. In this way, the effect of the time-dependent intraband electric field can be incorporated into the calculation of the interband polarization, which is directly related to the optical absorption.

To demonstrate that the changes in the nonlinear absorption spectra with density can be used to determine the intraband electric field in the BSSL, we plot in Fig. 3(b) the *linear* absorption spectra calculated using Eq. (16) for different *external* dc bias fields. These external dc fields are chosen by subtracting the averaged self-induced dc fields obtained from intraband polarizations corresponding to different exciton densities from the applied dc electric field F_o, which is 11.5 kV/cm. Because the self-induced dc fields decay due to the limited exciton lifetime, we estimate the average bias field F' present during the pulse transit by adding to F_o the extrapolation of the average intraband field back to a time $\simeq 0.15$ ps. This is indicated by the stars in Fig. 2. The lines roughly give the quasi-dc component of the intraband field, with the Bloch oscillations averaged out. From the strong similarity between the absorption spectra in Figs. 3(a) and 3(b), we see that the key features of the absorption peak shifts of the nonlinear absorption spectra in Fig. 3(a) primarily arise from the change in the internal electric field in the BSSL. This is what we call the *quasistatic approximation*: the system responds as if it is in a field given by the average field present shortly (0.1–0.3 ps) after the optical pulse arrives. Thus the nonlinear absorption can be used to estimate the average intraband field present just after the optical pulse arrives at the sample.

The small deviations of Fig. 3(b) from Fig. 3(a) arise partially from the errors in estimating the appropriate average self-induced electric fields from intraband polarizations. More importantly, because the self-induced electric field is time dependent during and after the excitation process, it cannot be entirely replaced by a modified static field F'. This approximation is quite good for the densities examined here. However, as has been shown in our earlier work,[53] if the internal intraband field has a large component at frequencies near the BO frequency, then these THz photons will stimulate transitions between WSL levels. This leads to a more complicated nonlinear absorption spectra that cannot simply be explained in the quasistatic approximation. For the densities shown, even though the wave packets are clearly undergoing rather strong BO's, the power at the BO frequency is not large enough relative to the dc component to make this a large effect. However, we find that at higher densities (but not extremely high densities), these effects can be quite significant, especially in the higher-frequency range of the absorption spectrum.

The absorption spectra presented in Fig. 3(a) are in the moderate-density regime. As the density is increased beyond this range, the quasistatic approximation begins to break down. We find that the quasistatic approximation is the poorest at densities near 1.2×10^{10} cm^{-2} (not shown), because at these densities, there is a definite WSL and the BO amplitude is large. However, we find that at very high densities ($>10^{10}$ cm^{-2}), the quasistatic approximation improves again due to the destruction of the WSL by the induced field. In Fig. 4, we plot the absorption spectrum at an excitation density of $\rho=13.8\times10^{10}$ cm^{-2} (solid line). Under such a strong excitation, the self-induced internal intraband electric field is so strong that it completely screens out the original applied dc field at early times (see inset to Fig. 4).[31] Thus the average net dc field in the BSSL is essentially zero while the optical pulse is present. Therefore, there is no WSL and hence essentially no BO's either. These features are seen in the inset to Fig. 4, where we have plotted the intraband field. The strong oscillations in the intraband field are not BO's, but rather are plasma oscillations, as we have discussed in an earlier publication.[31] The nonlinear absorption in this case is similar to the linear absorption of the BSSL with the biased field $F_o=0$ kV/cm. Choosing ΔE in Eq. (16) to be

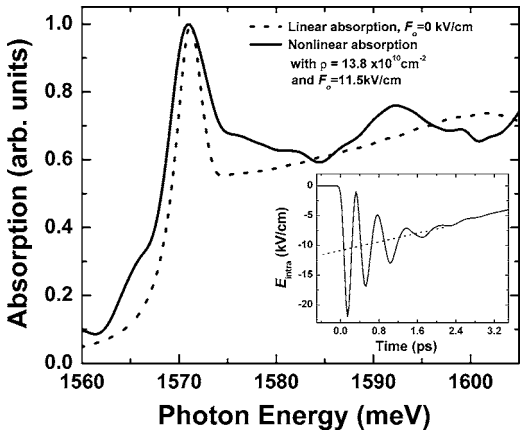

FIG. 4. Linear absorption spectrum (dashed line) with a bias field of $F_o=0$ kV/cm and nonlinear optical absorption spectrum (solid line) under strong excitation ($\rho=13.8\times10^{10}$ cm^{-2}) with a bias field of $F_o=11.5$ kV/cm. Inset: self-induced intraband field evolution for this excitation density.

3.87 meV, we plot the linear absorption for the zero-bias case in Fig. 4 (dotted line). The dominant absorption peak associated with the ground-state 1*s* exciton in the zero-bias linear spectrum and the nonlinear spectrum under the strong excitation are both at a similar energy of 1571 meV to within an error of 0.2 meV. However, unlike in low-density limit where the linear and nonlinear spectral peaks have same width, if we choose ΔE to be 3.87 meV (Fig. 1), the widths for the two spectral peaks are different in Fig. 4. The 1*s* peak is broadened in the nonlinear absorption spectra due to the fact that the excitons created at different times are created under quite different bias fields, as it takes time for the depolarization field to build up. There are relatively few complications arising from inter WSL transitions, because there is essential no WSL while the optical pulse is present. Surprisingly, the plasma oscillations do not seem to have a large effect on the position of the 1*s* excitonic peak. However, there are clearly strong perturbations at higher and lower frequencies that arise from these oscillations and the quasistatic approximation is not nearly as good as it was for the lower densities of Fig. 3.

We note that for the densities used in the results presented in Fig. 3, PSF effects can safely be neglected. However, for the large density presented in Fig. 4, it is clear that PSF effects will modify our results considerably. Most notably, PSF effects will introduce absorption saturation and hole burning, which are not captured in our model. Thus, the high-density results of Fig. 4 are only qualitative. However, it indicates that at high densities, the quasistatic approach is expected to be valid again and the average intraband field can be estimated from the nonlinear absorption spectrum.

IV. PUMP-PROBE SPECTROSCOPY

In this section, we employ Eqs. (6), (7), and (11) to simulate a pump-probe experiment. We will see that such a measurement allows us to deduce the *time dependence* of the intraband field in the BSSL from the probe absorption spectra. The pump pulse is a long Gaussian pulse with a temporal FWHM of 2.77 ps and a spectral FWHM of 0.19 THz (0.77 meV) centered on the $(-1,1)$ state (see the narrow spectral pulse in Fig. 1). The time-dependent self-induced intraband field is shown in Fig. 5(a). For simplicity, we set the exciton lifetime T_{1ex} to be infinity for the excitons generated by the pump pulse. This is not necessary, but simplifies the discussion. The exciton density created by the pump pulse is $\rho=0.67\times10^{10}$ cm^{-2}. Now we show that the time-dependent electric field generated by the long Gaussian pulse can be measured by probing the BSSL with a second weak, spectrally broad pulse. The spectral and temporal FWHM of this probe pulse are, respectively, 21 meV and 86 fs [see Figs. 1 and 5(a)]. This probe pulse is weak such that it only creates a density of $\rho=0.67\times10^{8}$ cm^{-2} (1% of the population produced by the pump pulse); it arrives with different time delays τ relative to the pump pulse.

Figure 5(b) shows the probe absorption spectra for three different time delays $\tau=-2.5$ ps, 0 ps, and 2.5 ps [marked by the three stars in Fig. 5(a)]. As the time delay increases, the magnitude of the self-induced electric field becomes larger and thus the net internal dc field within the BSSL becomes smaller. When probing at different time delays, the weak spectrally broad pulse encounters different net internal electric field in the BSSL and thus is absorbed in different ways as shown in Fig. 5(b). By measuring the WSL spacing in the absorption spectra for a given time delay, it is possible to estimate the self-induced electric field within the BSSL at

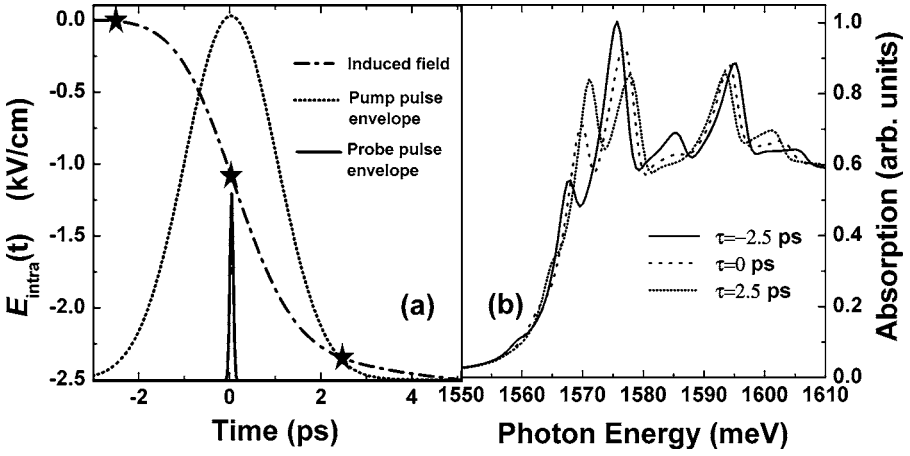

FIG. 5. (a). Self-induced intraband electric field (dash-dotted line) arising from the long Gaussian pulse (dotted line) with a temporal FWHM of 2.77 ps. Also shown is the ultrashort probe pulse (solid line). (b). Probe absorption spectra obtained at different time delays between the pump and probe pulses [marked by stars in (a)].

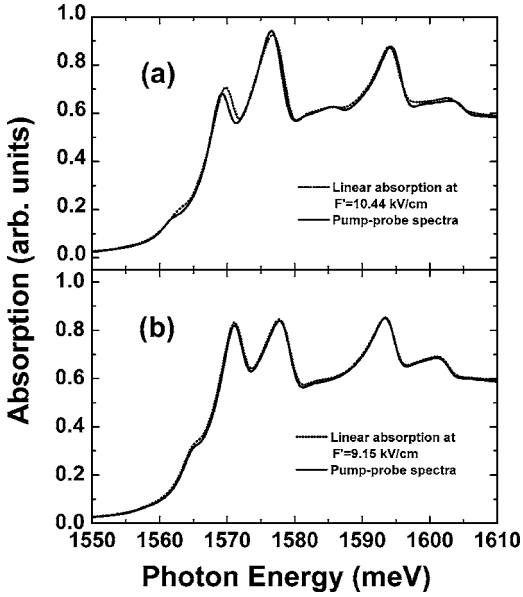

FIG. 6. (a) Comparison between the calculated pump-probe absorption spectra at time delay $\tau=0$ ps and the linear absorption spectra calculated with the corresponding net internal electric field of $F'=10.44$ kV/cm. (b) Comparison between the calculated pump-probe absorption spectra at time delay $\tau=2.5$ ps and the linear absorption spectra calculated with the corresponding net internal electric field, which is $F'=9.15$ kV/cm. The fields F' are given by the applied bias field plus the intraband field [Fig. 5(a)] present when the probe arrives.

this specific time. A more accurate estimate of the time-dependence of the intraband field can be obtained by comparing the pump-probe spectra directly with linear absorption spectra at different bias fields.

In Fig. 6, we plot the pump-probe absorption spectra for $\tau=0$ ps and 2.5 ps as well as the linear absorption spectra calculated using a bias field given by F_o plus the intraband field present at $t=\tau$ [see stars in Fig. 5(a)]. As can be seen, there is very good agreement between the two types of spectra, indicating that the pump-probe spectrum can be used to determine the time evolution of the intraband field. Note that the results agree better for $\tau=2.5$ ps than for $\tau=0$ ps. This is because the rate of change in the intraband field is much greater near $\tau=0$ ps than that near $\tau=2.5$ ps. In fact, improved agreement would be obtained for $\tau=0$ ps if the linear spectra were calculated with a field that is 0.32 kV/cm smaller than the 10.44 kV/cm field used. This is expected, because the probe pulse is not only sampling the system field for the 86 fs that it lasts; it produces an interband polarization that persists for roughly a time $T_{2inter}=0.34$ ps after the pulse has left. From Fig. 5(a), we see that the field is decreased by the required further 0.32 kV/cm at a time roughly 0.3 ps after the probe pulse arrives.

As with the nonlinear absorption technique, this quasistatic picture begins to break down if there are significant frequency components to the intraband field at the BO frequency. Such components are clearly very small for the long pump pulse considered here. However, if the pump pulse duration is reduced such that it generates BO wave packets (spectral FWHM greater than ω_B), then the THz-induced transitions will affect the probe spectrum and the quasistatic picture breaks down. This effectively puts a limit on the kinds of ultrafast internal field changes that can be probed using this technique: pump-probe spectroscopy can only be used in this system to directly measure internal intraband fields that do not have significant frequency components at the BO frequency. That is, the intraband fields cannot change by a large amount on time scales that are shorter than the BO period (0.43 ps for this system). This method can be used to map out the temporal evolution of the net bias field in a photoexcited BSSL or any other asymmetric multiple-quantum-well structure as long as this quasistatic approximation is valid.

V. CONCLUSIONS

In summary, we have used a nonperturbative excitonic formalism to investigate the nonlinear optical response of a BSSL. For single-pulse excitation, we calculated the ultrafast nonlinear optical absorption spectra of the BSSL. Pump-probe simulations were also performed to probe the time-dependent intraband field within the BSSL. We showed that the strong nonlinear optical response arises mainly from the self-induced intraband polarization and its strong interaction with the interband polarization. Our results show that as long as the time-dependent intraband field does not have a significant component at the BO frequency, then nonlinear absorption can be used to determine the peak intraband field in a BSSL excited by an ultrafast pulse and pump-probe spectroscopy can be used to determine the temporal evolution of the intraband field in a BSSL. We finally note that these two optical methods of probing the intraband field should also be directly applicable to asymmetric or biased quantum wells and coupled double quantum wells excited via an ultrafast optical pulse.

ACKNOWLEDGMENTS

The authors thank Ben Rosam and Karl Leo for insightful discussions. We would also like to thank Jean-Marc Lachaine for his critical contributions to the calculation of the excitonic basis. This work was supported in part by the Natural Sciences and Engineering Research Council of Canada.

[1] J. Shah, *Ultrafast Spectroscopy of Semiconductors and Semiconductor Nanostructures*, 2nd enlarged ed. (Springer, Berlin, 1999).
[2] T. Ando, J. Phys. Soc. Jpn. **66**, 1066 (1997).
[3] C. L. Kane and E. J. Mele, Phys. Rev. Lett. **90**, 207401 (2003).
[4] C. D. Spataru, S. Ismail-Beigi, L. X. Benedict, and S. G. Louie, Phys. Rev. Lett. **92**, 077402 (2004).
[5] E. Chang, G. Bussi, A. Ruini, and E. Molinari, Phys. Rev. Lett. **92**, 196401 (2004).
[6] T. G. Pederson, Carbon **42**, 1007 (2004).
[7] V. Perebeinos, J. Tersoff, and P. Avouris, Phys. Rev. Lett. **92**, 257402 (2004).
[8] M. M. Dignam and J. E. Sipe, Phys. Rev. Lett. **64**, 1797 (1990); Phys. Rev. B **43**, 4097 (1991).
[9] S. Glutsch and F. Bechstedt, Phys. Rev. B **60**, 16584 (1999).
[10] L. Yang, B. Rosam, J. M. Lachaine, K. Leo, and M. M. Dignam, Phys. Rev. B **69**, 165310 (2004).
[11] D. M. Whittaker, Europhys. Lett. **31**, 55 (1995).
[12] S. Glutsch and F. Bechstedt, Phys. Rev. B **57**, 11887 (1998).
[13] N. Linder, Phys. Rev. B **55**, 13664 (1997).
[14] C. P. Holfeld, F. Löser, M. Sudzius, K. Leo, D. M. Whittaker, and K. Köhler, Phys. Rev. Lett. **81**, 874 (1998).
[15] U. Behn, H. T. Grahn, K. Ploog, and H. Schneider, Phys. Rev. B **48**, 11827 (1993).
[16] S. Glutsch, D. S. Chemla, and F. Bechstedt, Phys. Rev. B **54**, 11592 (1994).
[17] D. S. Chemla and J. Shah, Nature (London) **411**, 549 (2001).
[18] V. M. Axt and S. Mukamel, Rev. Mod. Phys. **70**, 145 (1998).
[19] V. M. Axt and T. Kuhn, Rep. Prog. Phys. **67**, 433 (2004).
[20] T. Ando, A. B. Fowler, and F. Stem, Rev. Mod. Phys. **54**, 437 (1982).
[21] S. Schmitt-Rink, D. S. Chemla, and H. Haug, Phys. Rev. B **37**, 941 (1988).
[22] F. Rossi and E. Molinari, Phys. Rev. Lett. **76**, 3642 (1996); Phys. Rev. B **53**, 16462 (1996).
[23] F. Tassone and C. Piermarocchi, Phys. Rev. Lett. **82**, 843 (1999); C. Piermarocchi and F. Tassone, Phys. Rev. B **63**, 245308 (2001).
[24] S. Das Sarma and D. W. Wang, Phys. Rev. Lett. **84**, 2010 (2000).
[25] J. R. Madureira, M. H. Degani, and M. Z. Maialle, Phys. Rev. B **68**, 161301(R) (2003).
[26] H. Haug and S. W. Koch, *Quantum Theory of the Optical and Electronic Properties of Semiconductors*, 3rd ed. (World Scientific, Singapore, 1994).
[27] M. Załużny, J. Appl. Phys. **74**, 4716 (1993).
[28] M. Załużny, Phys. Rev. B **47**, 3995 (1993).
[29] K. Craig, B. Galdrikian, J. N. Heyman, A. G. Markelz, J. B. Williams, M. S. Sherwin, K. Campman, P. F. Hopkins, and A. C. Gossard, Phys. Rev. Lett. **76**, 2382 (1996).
[30] A. A. Batista and D. S. Citrin, Phys. Rev. Lett. **92**, 127404 (2004).
[31] L. Yang, B. Rosam, and M. M. Dignam, Phys. Rev. B **72**, 115313 (2005).
[32] H. M. James, Phys. Rev. **76**, 1611 (1949).
[33] G. H. Wannier, *Elements of Solid State Theory* (Cambridge University Press, Cambridge, England, 1959), p. 190.
[34] G. H. Wannier, Phys. Rev. **117**, 432 (1969).
[35] F. Bloch, Z. Phys. **52**, 555 (1928).
[36] C. Zener, Proc. R. Soc. London, Ser. A **145**, 523 (1934).
[37] F. Löser, M. M. Dignam, Yu. A. Kosevich, K. Köhler, and K. Leo, Phys. Rev. Lett. **85**, 4763 (2000).
[38] V. G. Lyssenko, G. Valusis, F. Löser, T. Hasche, K. Leo, M. M. Dignam, and K. Köhler, Phys. Rev. Lett. **79**, 301 (1997).
[39] M. Sudzius, V. G. Lyssenko, F. Löser, K. Leo, M. M. Dignam, and K. Köhler, Phys. Rev. B **57**, R12693 (1998).
[40] M. Hawton and M. M. Dignam, Phys. Rev. Lett. **91**, 267402 (2003).
[41] M. M. Dignam and M. Hawton, Phys. Rev. B **67**, 035329 (2003).
[42] F. Rossi and T. Kuhn, Rev. Mod. Phys. **74**, 895 (2002).
[43] S. Ben-Taboude-Leon and B. Laikhtman, Phys. Rev. B **67**, 235315 (2003).
[44] H. Haug and S. Schmitt-Rink, Prog. Quantum Electron. **9**, 3 (1984).
[45] S. Schmitt-Rink, C. Ell, and H. Haug, Phys. Rev. B **33**, 1183 (1986).
[46] G. Traetta, G. Col, and R. Cingolani, Phys. Rev. B **59**, 13196 (1999).
[47] D. Ninno, F. Liguori, V. Cataudella, and G. Iadonisi, J. Phys.: Condens. Matter **6**, 9335 (1994).
[48] P. Lipavský, V. Špička, and B. Velický, Phys. Rev. B **34**, 6933 (1986).
[49] G. Manzke, Q. Y. Peng, K. Henneberger, U. Neukirch, K. Hauke, K. Wundke, J. Gutowski, and D. Hommel, Phys. Rev. Lett. **80**, 4943 (1998).
[50] J. S. Nagerl, B. Stabenau, G. Bohne, S. Dreher, R. G. Ulbrich, G. Manzke, and K. Henneberger, Phys. Rev. B **63**, 235202 (2001).
[51] G. Manzke and K. Henneberger, Phys. Status Solidi B **234**, 233 (2002).
[52] L. J. Sham and T. M. Rice, Phys. Rev. **144**, 708 (1966).
[53] M. M. Dignam, Phys. Rev. B **59**, 5770 (1999).